



HYBRID PIEZOELECTRIC-INDUCTIVE AEROELASTIC ENERGY HARVESTER

José Augusto de Carvalho Dias

Carlos de Marqui Jr.

Department of Aeronautical Engineering, Engineering School of Sao Carlos, University of Sao Paulo, São Carlos, SP 13566-590, Brazil

guto.aero@gmail.com

demarqui@sc.usp.br

Abstract. *The use of linear and nonlinear aeroelastic vibrations for converting airflow energy into low-power electricity has received growing attention in the energy harvesting literature. The use of an aeroelastic typical section is a convenient approach to create persistent oscillations for energy harvesting. The main motivation is to power wireless electronic components located in high wind areas with potential applications ranging from aircraft structures to several engineering problems. Many researches on wind energy harvesting are using transduction mechanisms such as piezoelectric, electromagnetic or electrostatic separately to transform flow-induced vibrations into electricity. In this work, the concept of a hybrid airfoil-based aeroelastic energy harvester that simultaneously exploits piezoelectric transduction and electromagnetic induction is presented with electroaeroelastic modeling and simulations. The system has two degrees of freedom, pitch and plunge, and both forms of electromechanical coupling are introduced to the plunge degree of freedom. The effects of systems parameters on the total power output as well as on the linear and nonlinear piezoaeroelastic behavior are discussed. The results presented in this paper can be used for design and fabrication of optimal airfoil-based piezoelectric-inductive flow energy harvesters for the maximum electrical power output at reasonable low airflow speeds.*

Keywords: *Aeroelasticity, Energy Harvesting, Piezoelectricity, Electromagnetic Induction, Flow Excitation.*

1. INTRODUCTION

The main motivation in aeroelastic energy harvesting research is to enable scalable and low-profile flow energy harvesters. The goal is to power small electronic components for applications ranging from health monitoring (in aircraft or civil structures, for example) to wireless sensors located in high wind areas. The combination of aeroelastic vibrations with an appropriate transduction mechanism for transforming flow energy into low-power electricity has received growing attention in the energy harvesting literature. Two methods of creating persistent vibrations in flow energy harvester are the use of bluff-body based configurations or aeroelastic configurations. The first use of a piezoelectric interface in flow energy harvesting appears to be the bluff body – PVDF (polyvinylidene fluoride) membrane configuration tested under water by Allen and Smits (2001). The von Kármán vortex street formed behind the bluff body excites the piezoelectric PVDF to extract electricity from flow-induced vibrations through the direct piezoelectric effect. For the piezoaeroelastic problem of energy harvesting from airflow excitation of a cantilevered plate with embedded piezoceramics, De Marqui et al (2010a and 2010b) presented finite-element models based on the vortex-lattice method (De Marqui, 2010a) and the doublet-lattice method (2010b) of aeroelasticity (Bisplinghoff and Ashley, 1962). Time-domain simulations (De Marqui, 2010a) were given for a cantilevered plate with embedded piezoceramics for various airflow speeds below the linear flutter speed and at the flutter boundary. Frequency-domain simulations (De Marqui, 2010b) considering resistive and resistive-inductive circuits were also presented focusing on the linear response at the flutter boundary. Bryant and Garcia (2011) studied the aeroelastic energy harvesting problem for a typical section by using the finite state theory of Peters et al. (1995) while Erturk et al. (2010) presented an experimentally validated lumped-parameter model for a wing-section (airfoil) with piezoceramics attached onto plunge stiffness members using Theodorsen's unsteady aerodynamic model (Theodorsen, 1935). Piezoelectric power generation at the flutter boundary, including the minor shift in the linear flutter speed has also been discussed (Erturk et al., 2010). More recently the nonlinear version of the same setup (with a free play in the pitch degree-of-freedom) has been investigated to increase the operating envelope of the aeroelastic energy harvester (Sousa et al., 2011). In particular, hardening cubic nonlinearity and free play are combined to keep the oscillation amplitudes at an acceptable level while reducing the cut-in speed.

As an alternative to airfoil-based and cantilevered wing-based configurations, St. Clair et al. (2010) presented a design that uses a piezoelectric beam embedded within a cavity under airflow. Vortex-induced oscillations of piezoelectric cantilevers located behind bluff bodies were investigated by Poberinget al. (2009) and Akaydin et al. (2010) through experiments and numerical simulations. Giacomello and Porfiri (2011) investigated underwater flapping of an ionic polymer-metal composite (IPMC) flag. More recently Peterson and Porfiri (2012) studied the energy extraction mechanism from a vortex ring using an IPMC cantilever. Underwater base excitation of piezoelectric (Erturk

and Delporte, 2011) and IPMC (Aureli et al., 2010) cantilevers has also been investigated for low-power electricity generation.

An extensive analysis of the energy harvesting potential for a foil-damper system is presented by Peng and Zhu (2009) using a Navier-Stokes model without focusing on a specific transduction mechanism. Akcabay and Young (2012) investigated the energy harvesting potential of flexible beams in viscous flow along with the effects of system parameters. Tang et al. (2009) presented a rigorous analysis of the energy transfer from the fluid to the structure for self-excited vibrations due to axial flow over a cantilever. Piezoelectric energy harvesting from *LCO* under axial flow over a cantilever beam has also been discussed by Dunnmon et al. (2011) recently. Kwon (2010) considered a T-shaped cantilever beam that causes vortex street formation over the cantilever in response to axial flow. Kwuimy et al. (2012) employed a bi stable energy harvester (Erturk et al., 2009) for turbulent wind energy harvesting. Recent efforts have also employed electromagnetic induction for converting aeroelastic vibrations into electricity through flutter wake galloping (Jung and Lee, 2011) and bluff body-based oscillations (Zhu et al., 2010).

Piezoelectric conversion is convenient to employ for extracting energy from structural vibrations (e.g., from the strain fluctuations of a heaving plunge cantilever) by means of attaching piezoceramic patches while electromagnetic induction is useful for transforming relative motions (e.g., at the tip of the plunge cantilever relative to the ground) into electricity. Combination of these transduction mechanisms within a single hybrid flow energy harvester can improve the power density while employing the same simple platform. In the present work, a nonlinear airfoil-based aeroelastic energy harvester with pitch and plunge DOF is investigated. Piezoelectric transduction and electromagnetic induction are simultaneously considered and the system is analyzed based on fully coupled electroaeroelastic modeling. Both forms of electromechanical coupling are introduced to the plunge degree of freedom. Dimensionless electroaeroelastic equations are obtained to study the effects of certain parameters and geometric scaling of the hybrid piezoelectric-inductive energy harvester concept introduced herein.

2. ELECTROAEROELASTIC TYPICAL SECTION MODEL

Figure 1 shows the schematic of a two-degree-of-freedom (2-DOF) typical section. The plunge and pitch displacement variables are denoted by h and α , respectively. The plunge displacement is measured at the elastic axis (positive in the downward direction) and the pitch angle is measured about the elastic axis (positive in the clockwise direction). In addition, b is the semichord of the airfoil section, x_α is the dimensionless chord-wise offset of the elastic axis from the centroid (C), k_h is the stiffness per length in the plunge DOF, k_α is the stiffness per length in the pitch DOF, d_h is the damping coefficient per length in the plunge DOF, d_α is the damping coefficient per length in the pitch DOF, and U is the airflow speed.

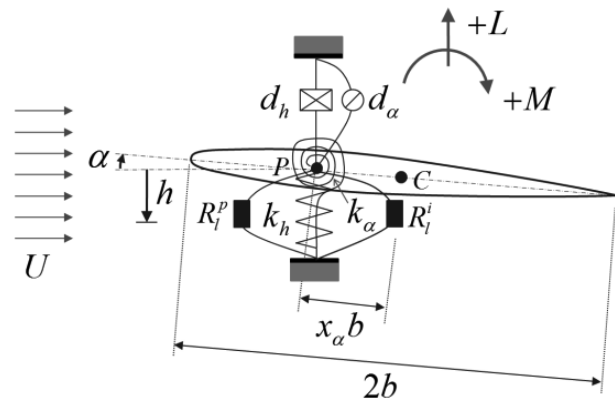


Figure 1. Electroaeroelastic typical section under airflow excitation with piezoelectric and inductive coupling.

In this work, piezoelectric coupling and electromagnetic induction are added to the plunge DOF of the typical section along with a resistive load for each electrical circuit, as shown in Fig. 1. The electroaeroelastically coupled equations governing the dynamics of hybrid (piezoelectric-inductive) flow energy harvester using a 2-DOF nonlinear typical section are

$$(m + m_e)\ddot{h} + mbx_\alpha\ddot{\alpha} + d_h\dot{h} + k_h h - \frac{\theta}{l}v - \frac{B_l}{l}I = -L \quad (1)$$

$$mbx_\alpha\ddot{h} + I_\alpha\ddot{\alpha} + d_\alpha\dot{\alpha} + f_a(\alpha)\alpha = M - f_b(\alpha) \quad (2)$$

$$C_p^{eq} \dot{v} + v/R_l^p + \theta \dot{h} = 0 \quad (3)$$

$$L_c \dot{I} + (R_c + R_l^i) I + B_l \dot{h} = 0 \quad (4)$$

where m is the airfoil mass per length (in the span direction), m_e is the fixture mass (connecting the airfoil to the plunge springs) per length, I_a is the airfoil moment of inertia, L is the aerodynamic lift, M is the aerodynamic moment. The over-dot represents differentiation with respect to time (t). The unsteady aerodynamic loads (lift and moment terms in Eqs. (1) and (2)) due to arbitrary motions are obtained from Jones' approximation (Jones, 1938) of Wagner's indicial function (Wagner, 1925), which is an approximation to the generalized Theodorsen function (Theodorsen, 1935). θ is the electromechanical coupling, B_l is the electromagnetic coupling, l is the span length, C_p^{eq} is the equivalent capacitance of the piezoceramic layers, R_l^p is the load resistance in the piezoelectric energy harvesting circuit, v is the voltage across the resistive load, L_c is the coil inductance, R_c is the internal resistance of the inductor coil, R_l^i is the load resistance in the inductive energy harvesting circuit, I is the induced electric current and

$$f_a(\alpha) = \begin{cases} k_\alpha & \text{If } \alpha < -\alpha_s \\ 0 & \text{If } -\alpha_s \leq \alpha \leq \alpha_s \\ k_\alpha & \text{If } \alpha > \alpha_s \end{cases} \quad (5)$$

$$f_b(\alpha) = \begin{cases} -k_\alpha \alpha_s & \text{If } \alpha < -\alpha_s \\ 0 & \text{If } -\alpha_s \leq \alpha \leq \alpha_s \\ k_\alpha \alpha_s & \text{If } \alpha > \alpha_s \end{cases} \quad (6)$$

where α_s is the modulus of the free play boundaries (for pitch angles ranging from $-\alpha_s$ to α_s the stiffness per length in the pitch DOF is neglected). Figure 2 show the experimentally difference between the measured linear and bilinear (free play) pitching moments used by Sousa et al. (2011).

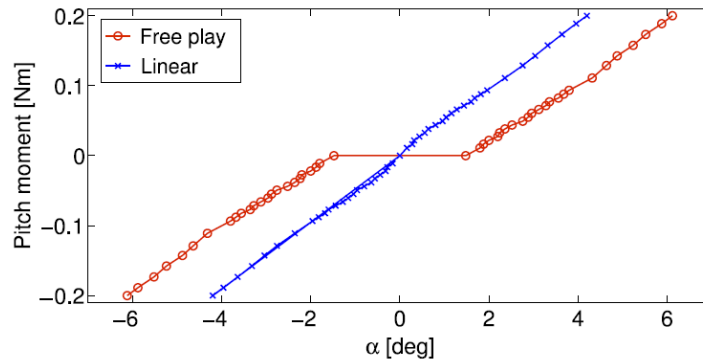


Figure 2. Restoring moments in the pitch DOF for the linear and the free play configurations used by Sousa et al. (2011).

Equations (1-4) can be written in dimensionless form as,

$$\beta \bar{h}'' + x_\alpha \bar{\alpha}'' + \zeta_h \bar{h}' + \bar{h} - \kappa \bar{v} - \chi \bar{I} = -\bar{L}_h \quad (7)$$

$$x_\alpha \bar{h}'' + \bar{r}_\alpha^2 \bar{\alpha}'' + \zeta_\alpha \bar{\alpha}' + \bar{f}_a(\alpha) \bar{\alpha} - \bar{f}_b(\alpha) = \bar{M}_\alpha \quad (8)$$

$$\eta \bar{v}' + \bar{v}/\lambda_l^p + \kappa \bar{h}' = 0 \quad (9)$$

$$\varphi \bar{I}' + \lambda_c \bar{I} + \lambda_l^i \bar{I} + \chi \bar{h}' = 0 \quad (10)$$

where $\beta = (m + m_e)/m$, $\bar{h} = h/b$ is the dimensionless plunge displacement, $\bar{\alpha} = \alpha/\alpha^*$ (where $\alpha^* = 1$ rad is the reference pitch angle), $\zeta_h = d_h/m\omega_h$ is the plunge damping ratio, $\zeta_\alpha = d_\alpha/m b^2\omega_h$ is the dimensionless pitch damping ratio, $\bar{r}_\alpha = r_\alpha/b$ is the dimensionless radius of gyration, $\bar{v} = v/v^*$ (where $v^* = 1$ V is the reference voltage), $\kappa = \theta v^*/l m b \omega_h^2$ is the dimensionless piezoelectric coupling, $\eta = C_p^{eq}(v^*)^2/m b^2 l \omega_h^2$ is the dimensionless equivalent capacitance, $\lambda_i^p = R_i^p m b^2 l \omega_h^3 / (v^*)^2$ is the dimensionless load resistance for the piezoelectric energy harvesting circuit, $\bar{I} = I/I^*$ (where $I^* = 1$ A is the reference current), $\chi = B_l I^*/l m b \omega_h^2$ is the dimensionless inductive coupling, $\varphi = L_c (I^*)^2 / l m b^2 \omega_h^2$ is the dimensionless inductance, $\lambda_i^i = R_i^i (I^*)^2 / l m b^2 \omega_h^3$ is the dimensionless load resistance for the inductive energy harvesting circuit, $\lambda_c = R_c (I^*)^2 / l m b^2 \omega_h^3$ is the dimensionless internal resistance, $\gamma = \omega_\alpha / \omega_h$ is the frequency ratio, $\omega_h^2 = k_h/m$ is the square of the plunge natural frequency, $\omega_\alpha^2 = k_\alpha/I_\alpha$ is the square of the pitch natural frequency. The dimensionless aerodynamic loads are $\bar{L} = L/m b \omega_h^2$ and $\bar{M} = M/m b^2 \omega_h^2$. In the governing equations, the prime (') denotes that the differentiation with respect to the dimensionless time $\tau = \omega_h t$. Also

$$\bar{f}_a(\alpha) = \begin{cases} \bar{r}_\alpha^2 \gamma_\alpha^2 & \text{If } \alpha < -\alpha_s \\ 0 & \text{If } -\alpha_s \leq \alpha \leq \alpha_s \\ \bar{r}_\alpha^2 \gamma_\alpha^2 & \text{If } \alpha > \alpha_s \end{cases} \quad (11)$$

$$\bar{f}_b(\alpha) = \begin{cases} -\bar{r}_\alpha^2 \gamma_\alpha^2 \alpha_s & \text{If } \alpha < -\alpha_s \\ 0 & \text{If } -\alpha_s \leq \alpha \leq \alpha_s \\ \bar{r}_\alpha^2 \gamma_\alpha^2 \alpha_s & \text{If } \alpha > \alpha_s \end{cases} \quad (12)$$

The coupled piezoaeroelastic equations can be written in the state-space form by introducing the electromechanical coupling in the model proposed by Edwards et al. (1979). Thus the voltage and current output in the piezoelectric circuit and in the inductive circuit respectively should be considered as two additional state variables. The state-space piezoaeroelastic equations in the matrix form are

$$\begin{bmatrix} \mathbf{I} & \mathbf{0} & \mathbf{0} & \mathbf{0} & \mathbf{0} \\ \mathbf{0} & \tilde{\mathbf{M}} & \mathbf{0} & \mathbf{0} & \mathbf{0} \\ \mathbf{0} & \mathbf{0} & \mathbf{I} & \mathbf{0} & \mathbf{0} \\ \mathbf{0} & \mathbf{0} & \mathbf{0} & \eta & \mathbf{0} \\ \mathbf{0} & \mathbf{0} & \mathbf{0} & \mathbf{0} & \varphi \end{bmatrix} \begin{bmatrix} \mathbf{x}' \\ \mathbf{x}'' \\ \mathbf{x}'_a \\ \bar{v}' \\ \bar{I}' \end{bmatrix} = \begin{bmatrix} \mathbf{0} & \mathbf{I} & \mathbf{0} & \mathbf{0} & \mathbf{0} \\ -\tilde{\mathbf{K}} & -\tilde{\mathbf{B}} & \mathbf{D} & \Theta_1 & X_1 \\ \mathbf{E}_1 & \mathbf{E}_2 & \mathbf{F} & \mathbf{0} & \mathbf{0} \\ \mathbf{0} & \Theta_2 & \mathbf{0} & 1/\lambda_i^p & \mathbf{0} \\ \mathbf{0} & X_2 & \mathbf{0} & \mathbf{0} & Z \end{bmatrix} \begin{bmatrix} \mathbf{x} \\ \mathbf{x}' \\ \mathbf{x}_a \\ \bar{v} \\ \bar{I} \end{bmatrix} \quad (13)$$

where $\mathbf{x} = \{\bar{\alpha} \ \bar{h}\}^t$, $\Theta_1 = \{0 \ \kappa\}^t$, $\Theta_2 = \{0 \ \kappa\}$, $X_1 = \{0 \ \chi\}^t$, $X_2 = \{0 \ \chi\}$, $Z = (\lambda_i^i + \lambda_c)$, $\mathbf{x}_a = \{x_1 \ x_2\}^t$ (describe the two augmented aerodynamic states) and \mathbf{I} is the 2×2 identity matrix. The superscript t stands for transpose. The mass, stiffness, and damping-related matrices in Eq. (13) are

$$\tilde{\mathbf{M}} = \mathbf{M} - \frac{\rho b^2}{m} \mathbf{M}_{nc} \quad (14)$$

$$\tilde{\mathbf{K}} = \mathbf{K} - \frac{\rho b^2}{m} \left(\frac{U}{b}\right)^2 \left(\mathbf{K}_{nc} + \frac{1}{2} \mathbf{RS}_1\right) \quad (15)$$

$$\tilde{\mathbf{B}} = \mathbf{B} - \frac{\rho b^2}{m} \left(\frac{U}{b}\right) \left(\mathbf{B}_{nc} + \frac{1}{2} \mathbf{RS}_2\right) \quad (16)$$

where \mathbf{M} is the structural mass matrix, \mathbf{B} is the structural damping matrix, \mathbf{K} is the structural stiffness matrix, ρ is the air density. \mathbf{M}_{nc} , \mathbf{B}_{nc} , and \mathbf{K}_{nc} are noncirculatory aerodynamic matrices related to inertia, damping and stiffness

respectively. These matrices as well as the aerodynamic matrices \mathbf{D} , \mathbf{E}_1 , \mathbf{E}_2 , \mathbf{F} , \mathbf{R} , \mathbf{S}_1 , and \mathbf{S}_2 can be found in Edwards et al (1979).

Equation (13) can be also represented as

$$\tilde{\mathbf{x}}' = \mathbf{A}\tilde{\mathbf{x}} \quad (17)$$

where

$$\mathbf{A} = \begin{bmatrix} \mathbf{0} & \mathbf{I} & \mathbf{0} & \mathbf{0} & \mathbf{0} \\ -\tilde{\mathbf{M}}^{-1}\tilde{\mathbf{K}} & -\tilde{\mathbf{M}}^{-1}\tilde{\mathbf{B}} & \tilde{\mathbf{M}}^{-1}\mathbf{D} & \tilde{\mathbf{M}}^{-1}\Theta_1 & \tilde{\mathbf{M}}^{-1}X_1 \\ \mathbf{E}_1 & \mathbf{E}_2 & \mathbf{F} & \mathbf{0} & \mathbf{0} \\ \mathbf{0} & \frac{1}{\eta}\Theta_2 & \mathbf{0} & \frac{1}{\eta}\frac{1}{\lambda_l^p} & \mathbf{0} \\ \mathbf{0} & \frac{1}{\varphi}X_2 & \mathbf{0} & \mathbf{0} & \frac{1}{\varphi}Z \end{bmatrix} \quad (18)$$

$$\tilde{\mathbf{x}} = \{\mathbf{x} \quad \mathbf{x}' \quad x_a \quad \bar{v} \quad \bar{I}\}^t \quad (19)$$

3. CASE STUDIES

This section presents the effects of dimensionless radius of gyration \bar{r}_α , frequency ratio γ , chord-wise offset of the elastic axis from the centroid x_α and free play boundaries module α_s on the dimensionless total electrical power as well as the dimensionless LCO speed are investigated in the case of a typical section with hybrid piezoelectric-inductive transduction. The load resistances in each set of parameters were chosen to maximize power output. The cut-in speed of limit cycle oscillations (\bar{U}_{lco}) is obtained for each set of parameters by checking the time histories with increasing airflow speed. The power output is obtained from the time histories obtained at the cut-in speed of each set of dimensionless parameters.

The nominal aeroelastic parameters belong to the piezoaeroelastic experimental setup used by Sousa et al. (2011) shown in Table 1. The dimensionless piezoelectric coupling, electromagnetic coupling, and piezoelectric capacitance have the fixed values of $\kappa = 5.9 \times 10^{-6}$, $\chi = 0.0305$, and $\eta = 3.66 \times 10^{-9}$.

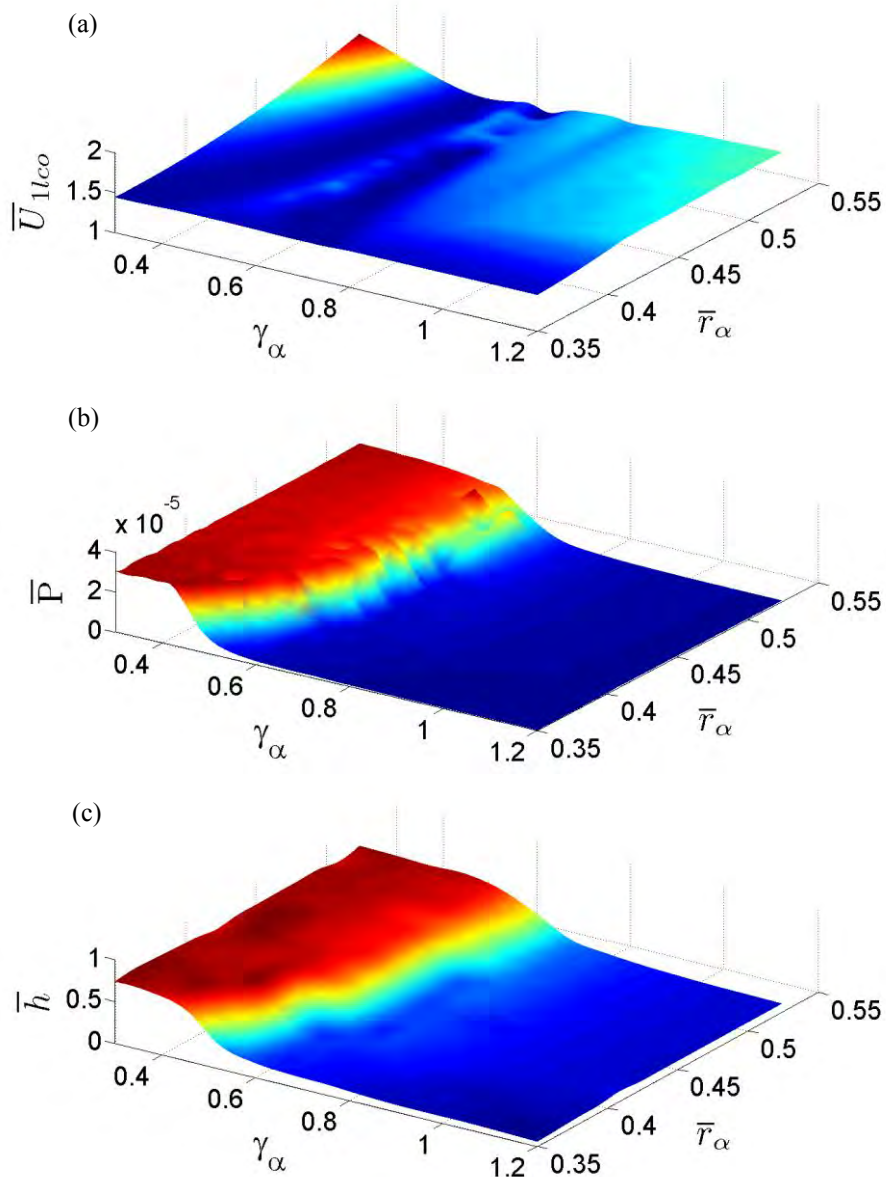
Table 1. Properties of the aeroelastic energy harvester.

β	2.5940
x_α	0.25
\bar{r}_α	0.5467
γ	0.5090
ζ_h	0.0535
ζ_α	0.1102
α_s	1.40

In the first case of study the effects of dimensionless radius of gyration (\bar{r}_α) and frequency ratio (γ) on the nonlinear aeroelastic behavior (cut-in speed of LCO) and power output are investigated. The variation of dimensionless cut-in speed ($\bar{U}_{lco} = U_{lco} / \omega_h b$) with \bar{r}_α and γ is displayed in Fig. 3a. The optimal electrical load resistance values of each set of aeroelastic parameters in both circuits (to maximize the power output) is considered and the fixed chord-wise offset of the elastic axis from the centroid is $x_\alpha = 0.25$ and fixed free play boundaries is $\alpha_s = 1.40$. The cut-in speed increases with increasing \bar{r}_α for all values of γ . Figure 3b shows the variation of total dimensionless electrical power output ($\bar{P} = \bar{v}^2 / \lambda_l^p + \bar{I}^2 \lambda_l^i$) with \bar{r}_α and γ for the dimensionless cut-in speed values of Fig. 3a. The electrical power output is higher at low frequency ratios, where the maximum plunge displacement occurs (as shown in Fig. 3c). The variation of pitch displacement is shown in Fig. 3d. For energy harvesting purposes the optimum set of parameters is obtained for the lowest values of radius of gyration and frequency ratio. This preferred condition corresponds to the configurations with the highest power output and the lowest cut-in speed. In Figs. 3a and 3b, the dimensionless load

Dias, J. A. C.; De Marqui, C.
Hybrid Piezoelectric-Inductive Aeroelastic Energy Harvester

resistance for the inductive energy harvesting circuit that generates maximum power output remains close to the value of dimensionless internal coil resistance, $(\lambda_l^i)_{optimal} \cong \lambda_c = 0.1022$ (in agreement with the maximum power transfer theorem, Agarwal and Lang, 2005) while the optimal electrical load of the piezoelectric energy harvesting circuit remains constant with the variation of γ and remains close to $(\lambda_l^p)_{optimal} \cong 4.3e8$ with the variation of \bar{r}_α .



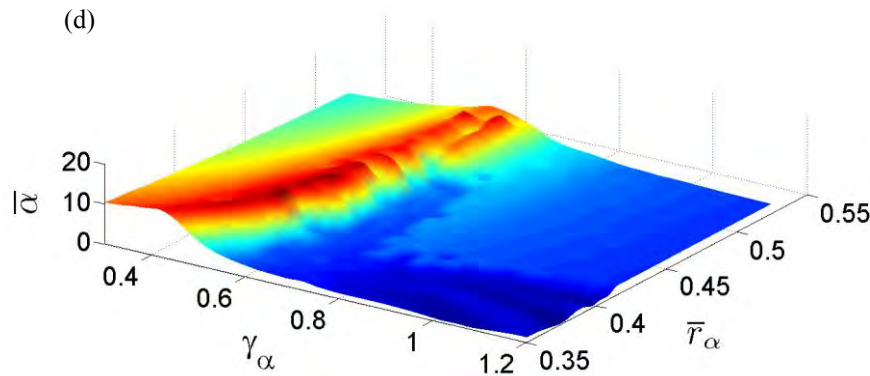
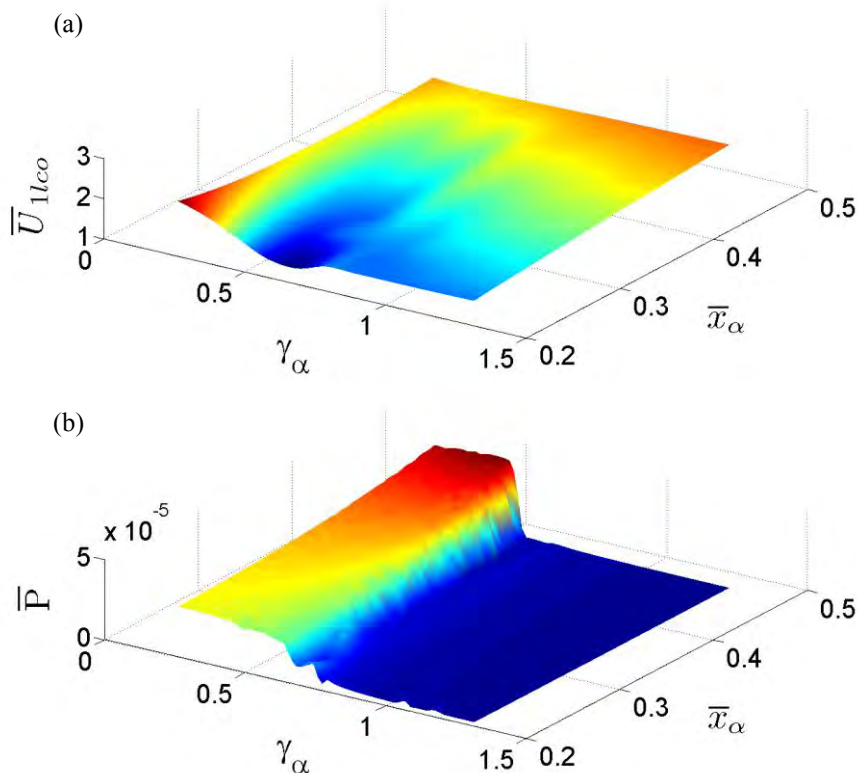


Figure 3. Dimensionless (a) cut-in speed, (b) power output, (c) plunge displacement and (d) pitch displacement versus dimensionless radius of gyration and frequency ratio (for a fixed chord-wise offset of the elastic axis from the centroid: $x_\alpha = 0.25$; and a fixed free play boundaries $\alpha_s = 1, 40$).

In the second case of study is the variation of cut-in speed of LCO and power output with the variation of dimensionless chord-wise offset of the elastic axis from the centroid (x_α) and frequency ratio (γ) is investigated. The variation of dimensionless cut-in speed (the lowest airflow speed where LCO is observed) with x_α and γ is displayed in Fig. 4a for the optimal electrical load resistance values (for each combination of aeroelastic parameters) in both circuits, fixed dimensionless radius of gyration ($\bar{r}_\alpha = 0.5467$) and fixed free play boundaries ($\alpha_s = 1.40$). The cut-in speed increases with increasing x_α (increasing the inertial coupling of the DOFs). Figure 4b shows the variation of total dimensionless electrical power output with x_α and γ obtained at each dimensionless airflow speed of Fig. 4a. The maximum total power output is obtained for the lowest γ and largest x_α as well as the maximum plunge displacement (that is shown in Fig. 4c). The variation of pitch displacement is shown in Fig. 4d. Once again, the optimal load resistance for the inductive energy harvesting circuit remains close to the value of dimensionless internal coil resistance ($(\lambda_q^i)_{optimal} \cong \lambda_c = 0.1022$) while the optimal electrical load of the piezoelectric energy harvesting circuit remains constant with the variation of γ and remains close to $(\lambda_q^p)_{optimal} \cong 4.3e8$ with the variation of \bar{r}_α .



Dias, J. A. C.; De Marqui, C.
Hybrid Piezoelectric-Inductive Aeroelastic Energy Harvester

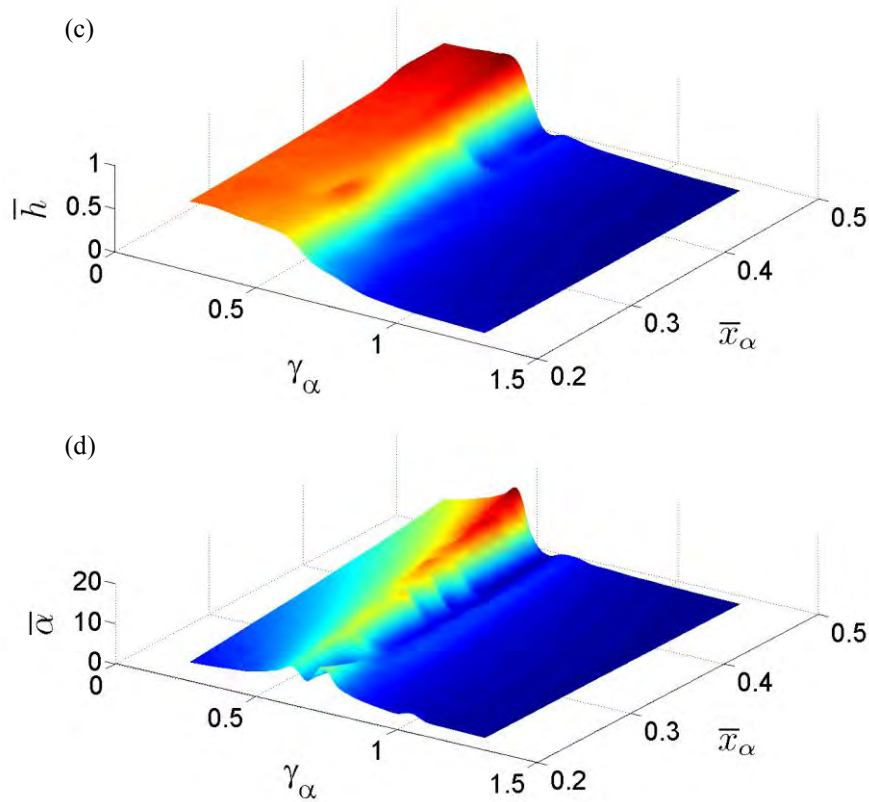


Figure 4. Dimensionless (a) cut-in speed, (b) power output, (c) plunge maximum displacement and (d) pitch maximum displacement versus dimensionless chord-wise offset of the elastic axis from the centroid and frequency ratio (for a fixed dimensionless radius of gyration: $\bar{r}_\alpha = 0.5467$; and a fixed free play boundaries $\alpha_s = 1, 40$).

In the third case of study is the variation of cut-in speed of LCO and power output with the variation of dimensionless free play boundaries (α_s) and frequency ratio (γ) is investigated. The variation of dimensionless cut-in speed with α_s and frequency ratio γ is displayed in Fig. 5a for the optimal electrical load resistance values (for each combination of aeroelastic parameters) in both circuits, fixed dimensionless radius of gyration ($\bar{r}_\alpha = 0.5467$) and fixed chord-wise offset of the elastic axis from the centroid ($x_\alpha = 0.25$). The airflow speed increases with increasing α_s for larger values of γ . For γ around 0.5, a region of minimum cut in speed is observed for all values of freeplay considered in the simulations. Figure 5b shows the variation of total dimensionless electrical power output with x_α and γ obtained at each dimensionless airflow speed of Fig. 5a. The electrical power output is larger at low frequency ratios, the region where maximum plunge displacement is also observed (shown in Fig. 5c). The variation of pitch displacement is shown in Fig. 5d. Once again, the optimal load resistance for the inductive energy harvesting circuit remains close to the value of dimensionless internal coil resistance ($(\lambda_i^i)_{optimal} \cong \lambda_c = 0.1022$) while the optimal electrical load of the piezoelectric energy harvesting circuit remains constant ($(\lambda_i^p)_{optimal} \cong 4.3e8$) with the variation of γ and α_s .

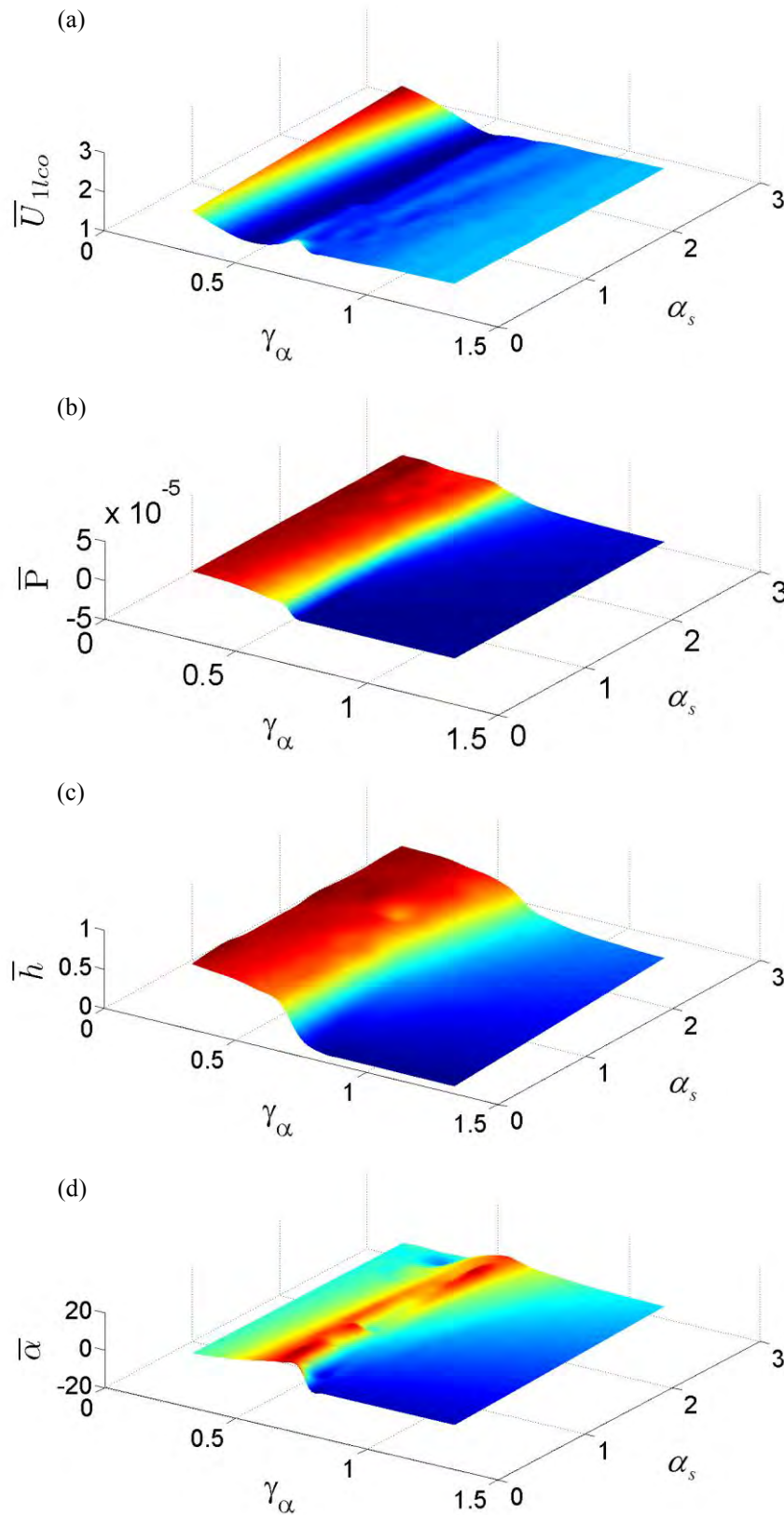


Figure 5. Dimensionless (a) cut-in speed, (b) power output, (c) plunge maximum displacement and (d) pitch maximum displacement versus dimensionless free play boundary modulus and frequency ratio (for a fixed dimensionless radius of gyration: $\bar{r}_\alpha = 0.5467$; and a fixed chord-wise offset of the elastic axis from the centroid: $x_\alpha = 0.25$).

4. CONCLUSIONS

The modeling and analysis of a nonlinear airfoil-based aeroelastic energy harvester using simultaneous piezoelectric transduction and electromagnetic induction is presented. The piezoelectric and electromagnetic coupling terms are introduced to the plunge DOF. The dimensionless governing equations are given with a resistive load in each electrical domain. The effects of several dimensionless system parameters (radius of gyration, chord-wise offset of the elastic axis from the centroid, free play boundaries module and frequency ratio) on the dimensionless electrical power as well as on the cut-in speed of LCOs are investigated.

The dimensionless cut-in speed decreases with decreasing radius of gyration, chord-wise offset of the elastic axis from the centroid and free play boundaries. The combination of low values of dimensionless radius of gyration and low values of frequency ratio, as well as large dimensionless chord-wise offset of the elastic axis from the centroid and free play boundaries increases the power output and keep low values of cut-in speed, which is a favorable condition for flow energy harvesters.

5. REFERENCES

- Agarwal, A. and Lang, J., 2005, *Foundations of Digital and Analog Electronic Circuits*, Morgan Kaufmann, San Francisco.
- Akaydin, H.D., Elvin, N. and Andreopoulos, Y., 2010, "Wake of a cylinder: a paradigm for energy harvesting with piezoelectric materials", *Experiments in Fluids*, 49, pp. 291-304.
- Akcabay, D.T. and Young, Y.L., 2012, "Hydroelastic response and energy harvesting potential of flexible piezoelectric beams in viscous flow", *Physics of Fluids*, 24, 054106.
- Allen, J.J. and Smits, A.J., 2001, "Energy Harvesting Eel", *Journal of Fluids and Structures*, 15, pp. 629-640.
- Amirtharajah, R. and Chandrakasan A.P., 1998, "Self-powered signal processing using vibration-based power generation", *IEEE Journal of Solid State Circuits*, 33, pp. 687-695.
- Aureli, M., Prince, C., Porfiri, M. and Peterson, S., 2010, "Energy Harvesting From Base Excitation of Ionic Polymer Metal Composites in Fluids Environments", *Smart Materials and Structures*, 19(1), 015003.
- Bisplinghoff, R. L. and Ashley, H., 1962, *Principles of Aeroelasticity*, John Wiley and Sons, New York.
- Bryant, M. and Garcia, E., 2011, "Modeling and Testing of a Novel Aeroelastic Flutter Energy Harvester", *ASME Journal of Vibration and Acoustics*, 133, 011010.
- De Marqui Jr., C., Erturk, A. and Inman, D.J., 2010a, "Piezoaeroelastic modeling and analysis of a generator wing with continuous and segmented electrodes", *Journal of Intelligent Material Systems and Structures*, 21, pp. 983-993.
- De Marqui Jr., C., Vieira, W.G.R., Erturk, A. and Inman, D.J., 2010b, "Modeling and Analysis of Piezoelectric Energy Harvesting from Aeroelastic Vibrations Using the Doublet-Lattice Method", *ASME Journal of Vibration and Acoustics*, 133, 011003.
- Dunnmon, J.A., Stanton, S.C., Mann, B.P., and Dowell, E.H., 2011. "Power extraction from aeroelastic limit cycle oscillations", *Journal of Fluids and Structures*, 27, pp. 1182-1198.
- Edwards, J.W., Ashley, H., and Breakwell, J.V., 1979, "Unsteady aerodynamic modeling for arbitrary motions", *AIAA Journal*, 17, pp. 365-374.
- Elvin, N. and Elvin, A., 2011, "An experimentally validated electromagnetic energy harvester", *Journal of Sound and Vibration*, 330, pp. 2314-2324.
- Erturk, A. and Delporte, G., 2011, "Underwater Thrust and Power Generation Using Flexible Piezoelectric Composites: An Experimental Investigation Toward Self-Powered Swimmer-Sensor Platforms", *Smart Materials and Structures*, 20, 125013.
- Erturk, A., Hoffmann, J., and Inman, D.J., "A piezomagnetoelastic structure for broadband vibration energy harvesting", *Applied Physics Letters*, 94, 254102.
- Erturk, A., Vieira, W.G.R., De Marqui, Jr., C. and Inman, D.J., 2010, "On the energy harvesting potential of piezoaeroelastic systems", *Applied Physics Letters*, 96, 184103.
- Giacomello, A. and Porfiri, M., 2011, "Underwater energy harvesting from a heavy flag hosting ionic polymer metal composites", *Journal of Applied Physics*, 109, 084903.
- Jones, R.T., 1938, "Operational treatment of the non-uniform-lift theory in airplane dynamics", *NACA Technical Report No. 667*.

22nd International Congress of Mechanical Engineering (COBEM 2013)
November 3-7, 2013, Ribeirão Preto, SP, Brazil

- Jung, H.J. and Lee, S.W., 2011, "The experimental validation of a new energy harvesting system based on the wake galloping phenomenon", *Smart Materials and Structures*, 20, 055022.
- Kwon, S.D., 2010, "A T-shaped piezoelectric cantilever for fluid energy harvesting", *Applied Physics Letters*, 77, 164102.
- Kwuimy, C.A., Litak, G., Borowiec, M., and Nataraj, C. 2012, "Performance of a piezoelectric energy harvester driven by air flow", *Applied Physics Letters*, 100, 024103.
- Peng, Z. and Zhu, Q., 2009, "Energy harvesting through flow-induced oscillations of a foil", *Physics of Fluids*, 21, 123602.
- Peters, D. A., Karunamoorthy, S., Cao, W. M., 1995, "Finite State Induced Flow Models; Dimensional Thin Airfoil", *Journal of Aircraft*, 32, pp. 313-322.
- Peterson, S. and Porfiri, M., 2012, "Energy exchange between a vortex ring and an ionic polymer metal composite", *Applied Physics Letters*, 100, 114102.
- Pobering, S., Ebermeyer, S. and Schwesinger, N., 2009, "Generation of electrical energy using short piezoelectric cantilevers in flowing media", *Proceedings of SPIE* 7288, 728807.
- Sousa, V.C., Anicézio, M., De Marqui, Jr., C., and Erturk, A., 2011, "Enhanced aeroelastic energy harvesting by exploiting combined nonlinearities: theory and experiment", *Smart Materials and Structures*, 20, 094007.
- St. Clair, D., Bibo, A., Sennakesavababu, V.R., Daqaq, M.F., Li, G., 2010, "A scalable concept for micropower generation using flow-induced self-excited oscillations", *Applied Physics Letters*, 96, 144103.
- Tang, L., Paidoussis, M. and Jiang, J., 2009, "Cantilevered flexible plates in axial flow: Energy transfer and the concept of flutter-mill", *Journal of Sound and Vibration*, 326, pp. 263-276.
- Theodorsen, T., 1935, "General theory of aerodynamic instability and the mechanism of flutter", *NACA Technical Report* No. 496.
- Wagner, H., 1925, "Über die Entstehung des dynamischen Auftriebes von Tragflügeln", *Zeitschrift für Angewandte Mathematik und Mechanik* 5, pp. 17-35.
- Zhu, D., Beeby, S., Tudor, J, White, N., and Harris, N., 2010, "A novel miniature wind generator for wireless sensing applications", *Proceedings of IEEE Sensors 2010*, pp. 1415-1418.

6. RESPONSIBILITY NOTICE

The authors are the only responsible for the printed material included in this paper.